

---

# Barlow Twins Deep Neural Network for Advanced 1D Drug–Target Interaction Prediction

---

Maximilian G. Schuh<sup>1</sup> Davide Boldini<sup>1,2</sup> Annkathrin I. Böhne<sup>3</sup> Stephan A. Sieber<sup>1</sup>

<sup>1</sup>Technical University of Munich, TUM School of Natural Sciences, Department of Bioscience, Center for Functional Protein Assemblies (CPA), Chair of Organic Chemistry II, 85748 Garching bei München, Germany

<sup>2</sup>Merck Healthcare KGaA, 64293 Darmstadt, Germany

<sup>3</sup>Technical University of Munich, TUM School of Natural Sciences, Department of Bioscience, Center for Functional Protein Assemblies (CPA), Chair of Biochemistry, 85748 Garching bei München, Germany

---

**Abstract** Accurate prediction of drug–target interactions is critical for advancing drug discovery. By reducing time and cost, machine learning and deep learning can accelerate this laborious discovery process. In a novel approach, BARLOWDTI, we utilise the powerful Barlow Twins architecture for feature-extraction while considering the structure of the target protein. Our method achieves state-of-the-art predictive performance against multiple established benchmarks using only one-dimensional input. The use of gradient boosting machine as the underlying predictor ensures fast and efficient predictions without the need for substantial computational resources. We also investigate how the model reaches its decision based on individual training samples. By comparing co-crystal structures, we find that BARLOWDTI effectively exploits catalytically active and stabilising residues, highlighting the model’s ability to generalise from one-dimensional input data. In addition, we further benchmark new baselines against existing methods. Together, these innovations improve the efficiency and effectiveness of drug–target interaction predictions, providing robust tools for accelerating drug development and deepening the understanding of molecular interactions. Therefore, we provide an easy-to-use web interface that can be freely accessed at <https://www.bio.nat.tum.de/oc2/barlowdti>.

---

## 1 Introduction

Studying drug–target interactions (DTIs) is crucial for understanding the biochemical mechanisms that govern how molecules interact with proteins.<sup>1</sup> Key challenges in drug discovery are the identification of proteins that can be used as targets for the treatment of diseases.<sup>2</sup> To achieve the desired therapeutic effects, the discovery of molecules that interact with and activate or inhibit target proteins is essential.<sup>3–5</sup>

Recent advances in computational methods have transformed the drug discovery landscape, providing robust tools for cost-effective exploration of the chemical space. These *in silico* approaches facilitate the prediction and analysis of DTIs, aiding in the identification of potential drug candidates and their corresponding protein targets.<sup>6–11</sup> The use of computational techniques allows researchers to gain a comprehensive understanding of the molecular mechanisms underlying DTIs, thereby accelerating the drug discovery process and minimising reliance on traditional, resource-intensive experimental methods.<sup>12,13</sup> Different methods have been used to understand how drugs interact with target proteins. These methods are grouped into three main categories: structure-agnostic, structure-based and complex-based.

Structure-agnostic approaches use one-dimensional (1D) representations like molecule simplified molecular-input line-entry system (SMILES) and protein amino acid sequences, or two-dimensional (2D) representations like graphs and predicted contact maps.<sup>14–17</sup> These methods

are cost-effective and sufficiently accurate compared to experimental or *in silico* structure prediction,<sup>18</sup> as they are independent of the protein’s structure when predicting effects.

Structure-based approaches require three-dimensional (3D) protein structures and 1D or 2D molecular inputs. 3D structures are usually derived from experimental data, although computational predictions are increasingly employed.<sup>19–23</sup> These methods have great potential but can be unreliable. They depend on accurate 3D protein structures and may be limited in their ability to generalise beyond experimentally observed DTIs.<sup>24</sup> Due to the complexity of the experimental setup, 3D protein structures can be difficult to obtain. In addition, models often overlook the fact that proteins are not rigid structures, but are generally in motion, e.g., ligand binding induces a conformational change.<sup>20,22,23</sup>

Finally, complex-based approaches require protein-ligand co-crystal structures, which additionally require 3D information, as well as protein interaction information about the ligand.<sup>25</sup> For this reason, complex-based approaches can provide a more detailed insight into the interactions, but they are by far the most difficult to obtain data for.

Considering these different approaches, we designed BARLOWDTI as a fully data-driven, sequence-based approach that relies on SMILES and amino acid sequences as the most accessible data, avoiding costly and time-consuming experimental data such as crystal structures. Additionally, we use a specialised bilingual protein language model (PLM) to embed the 1D amino acid sequence, which uses a 3D-alignment method that results in a “structure-sequence” representation.<sup>26,27</sup> This approach makes BARLOWDTI input data structure-agnostic, yet benefits from “structure-sequence” PLM embeddings. Unlike most other methods, we have developed a system that uses a hybrid “best of both worlds” machine learning (ML) and deep learning (DL) approach to improve DTI prediction performance in low data regimes where training data is limited.<sup>28,29</sup> We have found that DL architectures such as Barlow Twins<sup>30,31</sup> are excellent at learning features<sup>29</sup> that can then be used for gradient boosting machine (GBM) training to achieve state-of-the-art performance, as the size of datasets is usually too small to reliably train a DL model that will perform competitively.

To overcome the limitation of data scarcity, we built BARLOWDTI<sub>XXL</sub>, which is trained on millions of curated DTI pairs,<sup>32</sup> to apply the model to real-world examples, as we have done in case studies. Here, BARLOWDTI<sub>XXL</sub> captures the correlation between experimentally determined affinities and the predicted likelihood of interaction, proving our approach useful in drug discovery settings. By comparing co-crystal biochemical structures and their active sites, we also investigate and explain how BARLOWDTI<sub>XXL</sub> arrives at its decision. We conduct our investigation by employing an influence method and adapting it in a novel way to identify the most important training DTIs.<sup>33</sup> This work culminates in a freely available web interface that takes 1D input of molecule and protein information and predicts the likelihood of interaction.

## 2 Results and Discussion

**BARLOWDTI design.** We propose a novel method for predicting DTIs using SMILES notations, primary amino acid sequences, both 1D, and annotated interaction properties. BARLOWDTI relies on a several key components, visualised in Fig. 1:

1. Firstly, the input needs to be vectorised. This is achieved by converting SMILES to an extended-connectivity fingerprint (ECFP). The amino acid sequences are processed by a PLM that uses both modalities, combining 1D protein sequences and 3D protein structure.<sup>26</sup>
2. Secondly, we teach the self-supervised learning (SSL) based Barlow Twins model interaction of molecule and protein without considering labels.<sup>30,31</sup> The objective function implements invariance of both representation of one interaction while ensuring non-redundancy of the features.<sup>30,31</sup>

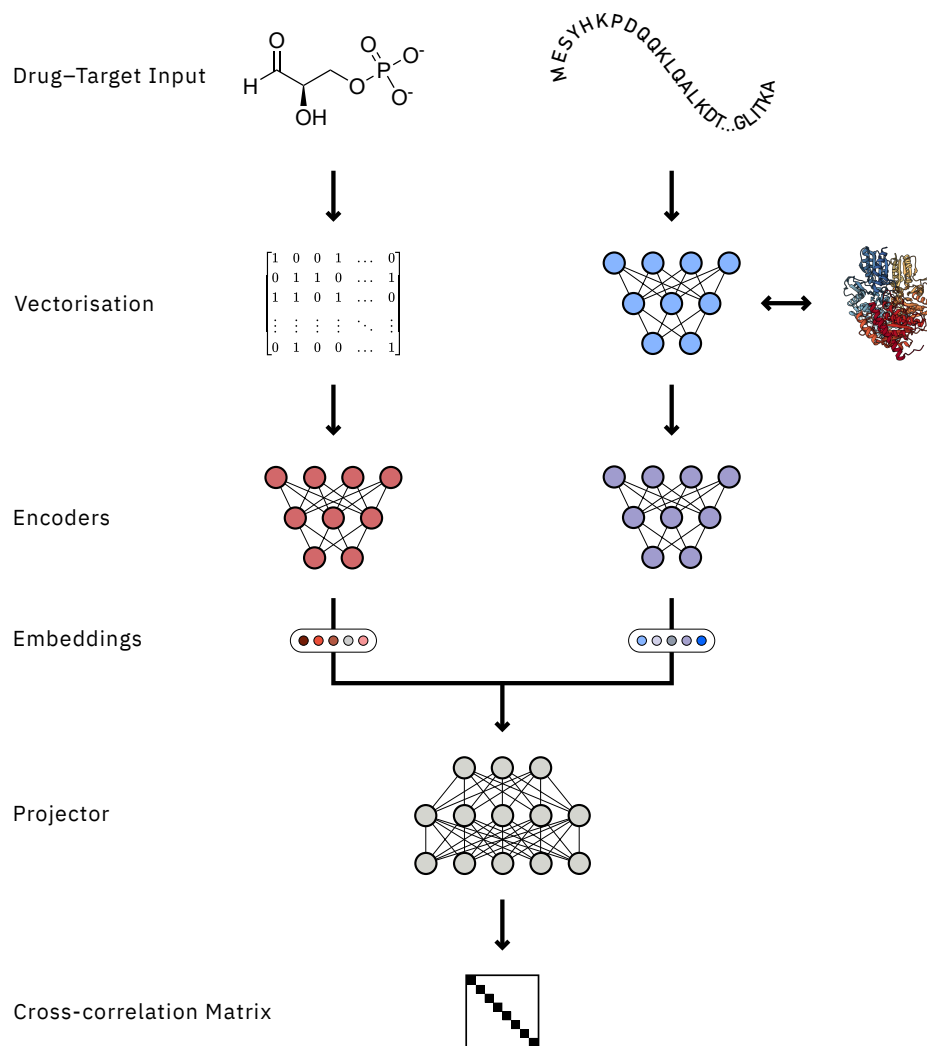


Figure 1: **BARLOWDTI architecture.** Drug and target serve as 1D input, where they are processed and converted into vectors. Molecules are provided as SMILES and converted to ECFP. On the other hand, the primary amino acid sequence is vectorised using a bilingual 3D structure-aware PLM. The Barlow Twins architecture learns to understand DTIs. The objective function forces both representations of the DTI to be as close as possible to the unity matrix. Finally, this DL model is used as a feature-extractor and a GBM is trained on the embeddings and the interaction label. The GBM is then used as the predictor.

- Finally, BARLOWDTI takes a combination of embeddings generated by the encoders from the Barlow Twins DL model and uses them as features to train a GBM based on the interaction annotations.<sup>28</sup> This approach exploits two key strengths: it uses DL to refine representations, and it leverages the power of ML in scenarios with limited data. This is particularly relevant for current DTI benchmarks/datasets, where only around 50 000 annotated pairs are publicly available.<sup>34–37</sup> Consequently, we propose BARLOWDTI<sub>XXL</sub> which is trained on more than 3 600 000 curated DTI pairs, additionally sourced from PubChem and ChEMBL,<sup>38,39</sup> to obtain generalisability in real-world scenarios.<sup>32</sup>

**Benchmark selection.** We selected a comprehensive set of literature-based benchmarks to evaluate the performance of BARLOWDTI against several leading methods. The benchmarks considered in

this study are derived from several key sources. These sources include biomedical networks,<sup>34</sup> the US patent database,<sup>35</sup> and data detailing the interactions of 72 kinase inhibitors with 442 kinases, representing over 80 % of the human catalytic protein kinome.<sup>36</sup> These datasets provide DTIs as pairs of molecules and amino acid sequences, each coupled to an interaction annotation.

To ensure a fair comparison, BARLOWDTI was retrained across all benchmarks. Finally, we assessed the model’s performance in a binary classification setting, where the task is to distinguish between interacting and non-interacting drug–target pairs:

- We compared BARLOWDTI with a total of seven established DTI models: the model by Kang et al., MolTrans,<sup>41</sup> DLM-DTI,<sup>17</sup> ConPLex,<sup>42</sup> DrugBAN,<sup>43</sup> PSICHIC,<sup>16</sup> and STAMP-DTI.<sup>44</sup> For instance, Kang et al. fine-tuned a large language model (LLM) based on amino acid sequences.<sup>40</sup> MolTrans uses an efficient transformer architecture to increase the scalability of the model.<sup>41</sup> DLM-DTI introduced a dual language model approach combined with hint-based learning to improve prediction accuracy.<sup>17</sup> ConPLex leveraged contrastive learning to better understand DTIs,<sup>42</sup> while DrugBAN focused on interpretable attention mechanisms that provide insights into the interaction process.<sup>43</sup> PSICHIC utilised physicochemical properties to predict interactions more accurately,<sup>16</sup> and STAMP-DTI incorporated structure-aware, multi-modal learning to enhance its predictive capabilities.<sup>44</sup> Overall, we evaluated our architecture against the various model implementations. These models – structure-agnostic, structure-based or complex-based – have demonstrated state-of-the-art performance in benchmarks.
- This comparison is performed on a total of four datasets with twelve literature-proposed splits: 4 × BioSNAP,<sup>16,34,40</sup> 4 × BindingDB,<sup>16,35,40</sup> 1 × DAVIS<sup>36,40</sup> and 3 × Human.<sup>16,41</sup> Our aim is to investigate the behaviour of different methods in diverse splitting scenarios, where a whole dataset is split into model training, validation, and evaluation subsets. These predefined splits help us to assess how well models generalise under challenging evaluation conditions, for example where either the drug or the target has not been seen before, thus providing insight into their real-world applicability.
- In addition, we investigated the addition of a more rigorous model baseline. The GBM XGBoost is known to be one of the best models, e.g. in quantitative structure–activity relationship (QSAR) tasks, often outperforming DL-based approaches.<sup>45–47</sup>

**BARLOWDTI shows state-of-the-art performance in predicting DTIs.** We assessed the performance of BARLOWDTI in binary classification across four distinct datasets, each employing different data splitting procedures. For each dataset, we predicted whether drug–target pairs in the predefined test subset interact or not. We then statistically evaluated these predictions by comparing them to the actual outcomes provided in the benchmark test set, using the metrics receiver operating characteristic area under curve (ROC AUC) and precision recall area under curve (PR AUC). Overall, BARLOWDTI significantly outperforms all other models in Fig. 2a and Tabs. 1 and 5. Looking at BioSNAP, we improve 6 % over the leading method DLM-DTI in terms of PR AUC. Furthermore, as shown in Tab. 2 BARLOWDTI again outperforms the PSICHIC method with a 7 % PR AUC improvement independent of the split.

When switching to BindingDB, BARLOWDTI significantly outperforms DLM-DTI in terms of PR AUC with a >14 % improvement (Tab. 1). Investigating the BindingDB splits shows that BARLOWDTI outperforms all existing methods when looking at unseen ligands, matches the ROC AUC performance of DrugBAN in the random setting and becomes second best in the unseen protein split (Tab. 2). Overall, BARLOWDTI performs best in two out of four splits in this benchmark.

BARLOWDTI once again outperforms all of the established approaches when looking at the DAVIS benchmark, with a 21 % improvement over the leading ConPLex model in terms of PR AUC (Tab. 1).

Table 1: **Benchmarking BARLOWDTI against other models using Kang et al. splits.**<sup>40</sup> Performance was evaluated against three established benchmarks, and the mean and standard deviation of the performance of five replicates are presented. Results per benchmark that are both the best and statistically significant (Two-sided Welch’s  $t$ -test,<sup>48,49</sup>  $\alpha = 0.001$  with Benjamini-Hochberg<sup>50</sup> multiple test correction) are highlighted in bold.

Dataset	Model	ROC AUC	PR AUC
BioSNAP	BARLOWDTI	<b>0.9599 ± 0.0004</b>	<b>0.9670 ± 0.0004</b>
	XGBoost	0.9142	0.9229
	MolTrans <sup>41</sup>	0.895 ± 0.002	0.901 ± 0.004
	Kang et al.	0.914 ± 0.006	0.900 ± 0.007
	DLM-DTI <sup>17</sup>	0.914 ± 0.003	0.914 ± 0.006
	ConPLex <sup>42</sup>	–	0.897 ± 0.001
BindingDB	BARLOWDTI	<b>0.9364 ± 0.0003</b>	<b>0.7344 ± 0.0018</b>
	XGBoost	0.9261	0.6948
	MolTrans <sup>41</sup>	0.914 ± 0.001	0.622 ± 0.007
	Kang et al.	0.922 ± 0.001	0.623 ± 0.010
	DLM-DTI <sup>17</sup>	0.912 ± 0.004	0.643 ± 0.006
	ConPLex <sup>42</sup>	–	0.628 ± 0.012
DAVIS	BARLOWDTI	<b>0.9480 ± 0.0008</b>	<b>0.5524 ± 0.0011</b>
	XGBoost	0.9285	0.4782
	MolTrans <sup>41</sup>	0.907 ± 0.002	0.404 ± 0.016
	Kang et al.	0.920 ± 0.002	0.395 ± 0.007
	DLM-DTI <sup>17</sup>	0.895 ± 0.003	0.373 ± 0.017
	ConPLex <sup>42</sup>	–	0.458 ± 0.016

Lastly, we evaluated the performance on the Human benchmark. BARLOWDTI shows the best performance when looking at the unseen protein split as well as the random split (Tab. 2). PSICHIC comes first in the unseen ligand setting, when looking at ROC AUC, while DrugBAN is best in PR AUC. In summary, BARLOWDTI outperforms all other models in two out of three splits.

We looked at the architecture and its components, removing one at a time and measuring the effect on performance to investigate why BARLOWDTI outperforms other methods in various benchmarks.

**Unravelling the performance contributions of the BARLOWDTI architecture.** To investigate the impact of each element of the BARLOWDTI architecture, we removed them one at a time. We have done this across all baselines and splits with the following ablations:

1. We removed the hyperparameter optimisation step of the BARLOWDTI classifier.
2. From the first removal, we replaced the Barlow Twins architecture entirely and instead concatenate ECFPs and PLM embeddings for training. We kept the hyperparameter optimisation procedure as in BARLOWDTI.
3. Finally, we removed the hyperparameter optimisation procedure from the previous ablation, analogous to the first modification.

We observe a significant decline in performance, as illustrated in Fig. 2b and Tab. 6 for the initial ablation, emphasising the crucial role of hyperparameter optimisation for achieving optimal model performance.

Table 2: **Benchmarking BARLOWDTI against other models using Koh et al. splits.**<sup>16</sup> Performance was evaluated against three established benchmarks, and the mean of the BARLOWDTI performance of five replicates are presented. All other metrics are taken from Koh et al.. Best result per benchmark and split is highlighted in bold. (Koh et al. does not present replicates or sample-correlated predictions.<sup>16</sup>)

Dataset	Split	Model	ROC AUC	PR AUC
BioSNAP	Unseen protein	BARLOWDTI	<b>0.9572</b>	<b>0.9679</b>
		DrugBAN <sup>16,43</sup>	0.7327	0.7971
		PSICHIC <sup>16</sup>	0.8819	0.9071
		STAMP-DPI <sup>16,44</sup>	0.8372	0.8738
		XGBoost	0.8506	0.8794
	Random split	BARLOWDTI	<b>0.9718</b>	<b>0.9755</b>
		DrugBAN <sup>16,43</sup>	0.9089	0.9159
		PSICHIC <sup>16</sup>	0.9246	0.9226
		STAMP-DPI <sup>16,44</sup>	0.8993	0.9056
		XGBoost	0.9146	0.9242
	Unseen ligand	BARLOWDTI	<b>0.9666</b>	<b>0.9706</b>
		DrugBAN <sup>16,43</sup>	0.8775	0.8843
		PSICHIC <sup>16</sup>	0.9019	0.9030
		STAMP-DPI <sup>16,44</sup>	0.8902	0.8915
		XGBoost	0.8909	0.9026
BindingDB	Unseen protein	BARLOWDTI	0.6939	0.5791
		DrugBAN <sup>16,43</sup>	0.6523	0.5295
		PSICHIC <sup>16</sup>	<b>0.7537</b>	<b>0.6241</b>
		STAMP-DPI <sup>16,44</sup>	0.6828	0.5735
		XGBoost	0.6460	0.5233
	Random split	BARLOWDTI	<b>0.9640</b>	0.9513
		DrugBAN <sup>16,43</sup>	<b>0.9640</b>	<b>0.9539</b>
		PSICHIC <sup>16</sup>	0.9503	0.9280
		STAMP-DPI <sup>16,44</sup>	0.9318	0.9085
		XGBoost	0.9582	0.9462
	Unseen ligand	BARLOWDTI	<b>0.9456</b>	<b>0.9263</b>
		DrugBAN <sup>16,43</sup>	0.9409	0.9188
		PSICHIC <sup>16</sup>	0.9264	0.8975
		STAMP-DPI <sup>16,44</sup>	0.9027	0.8683
		XGBoost	0.9374	0.9141
Human	Unseen protein	BARLOWDTI	<b>0.9630</b>	<b>0.9693</b>
		DrugBAN <sup>16,43</sup>	0.9298	0.9417
		PSICHIC <sup>16</sup>	0.9503	0.9595
		STAMP-DPI <sup>16,44</sup>	0.8563	0.8748
		XGBoost	0.8961	0.9171
	Random split	BARLOWDTI	<b>0.9917</b>	<b>0.9905</b>
		DrugBAN <sup>16,43</sup>	0.9841	0.9753
		PSICHIC <sup>16</sup>	0.9861	0.9840
		STAMP-DPI <sup>16,44</sup>	0.9659	0.9582
		XGBoost	0.9813	0.9782
	Unseen ligand	BARLOWDTI	0.9346	0.9348
		DrugBAN <sup>16,43</sup>	0.9459	<b>0.9387</b>
		PSICHIC <sup>16</sup>	<b>0.9500</b>	0.9371
		STAMP-DPI <sup>16,44</sup>	0.9156	0.8980
		XGBoost	0.9391	0.9337

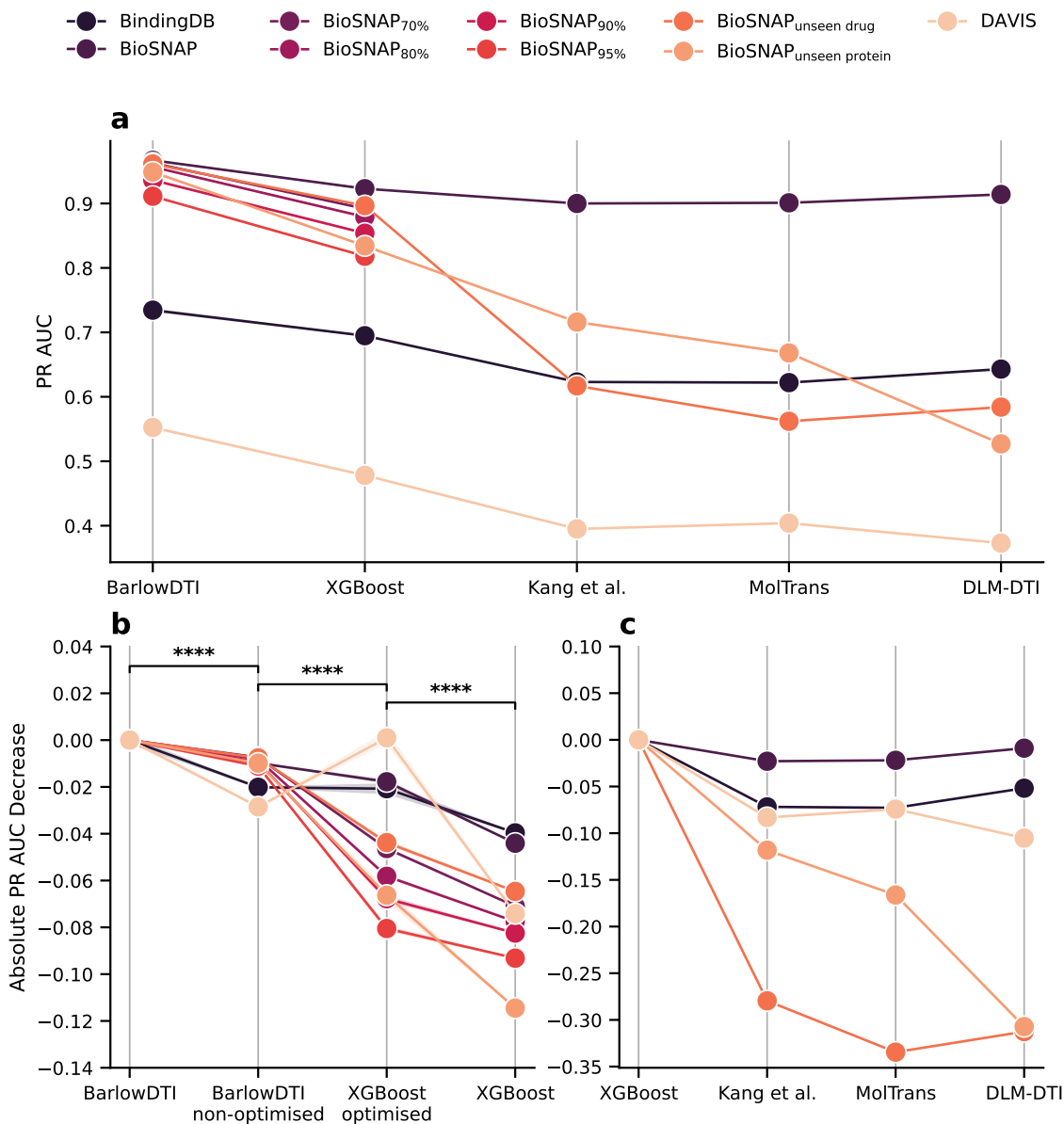


Figure 2: A comparison of the performance of methods established in the literature. a) The state-of-the-art performance of BARLOWDTI in terms of PR AUC was visualised in comparison to other models (for metrics and their statistics refer to Tab. 1). b) The change in performance was examined as key elements of the BARLOWDTI architecture were incrementally removed. c) The newly introduced model baseline, XGBoost, was compared with other established methods. A per dataset and split difference in PR AUC was calculated based on BARLOWDTI (in b) performance or the baseline model (in c). The overall change was investigated for statistical significance (\*\*\*\* $p < 0.0001$ , two-sided Welch's  $t$ -test,<sup>48,49</sup> with Benjamini-Hochberg<sup>50</sup> multiple testing correction).

The second ablation also indicates a significant reduction in performance. This is likely attributed to the DL architecture based on the SSL Barlow Twins model, which effectively learns embeddings to describe DTIs. The Barlow Twins objective promotes orthogonality between drug and target modalities while ensuring the non-redundancy of both, thus preventing informational collapse. As a result, this leads to an overall state-of-the-art predictive performance.

The final ablation shows a further decline in performance, consistent with the results of the initial ablation experiment.

In summary, the sustained reduction in performance of our ablation experiments demonstrates that each component of our BARLOWDTI pipeline is needed to maximise performance. This architecture integrates the “best of both worlds”: DL and GBM to enhance predictive performance. Compared to other pure ML- or DL-based approaches, we can demonstrate a performance boost. In particular, the use of a state-of-the-art PLM<sup>26</sup> could offer an advantage over other methods. Other PLM variants are ProtTrans T5<sup>51</sup> in ConPLex<sup>42</sup> and ProtBERT proposed by Kang et al. also used in DLM-DTI.<sup>40</sup> The structural awareness of BARLOWDTI added by the inclusion of 3D-alignment in ProstT5<sup>26</sup> hints towards better generalisation capabilities, yielding increased performance.

**Choosing baseline models** Selecting an appropriate baseline model is critical to effectively comparing different ML and DL techniques. Robust baselines are the basis for meaningful comparisons and highlight improvements from new methods. Without appropriate baselines, it becomes difficult to determine whether new approaches are truly advancing the field.

Current leading DTI models predominantly use DL methods and are often evaluated against simple baseline models such as logistic regression, ridge or deep neural network (DNN) classifiers.<sup>41,42</sup> To improve the benchmarking process, we propose to add GBMs as a baseline for DTI benchmarking purposes, as shown in the final ablation configuration. GBMs such as XGBoost have demonstrated broad adaptability, e.g. in QSAR modelling, offering strong predictive performance and fast training times, particularly in scenarios with limited data availability, such as DTI prediction.

We compared the overall model performance across all datasets in Fig. 2c and Tabs. 1, 2 and 7. Here, the performance of XGBoost trained on ECFPs and PLM embeddings is highlighted as it shows competitive performance across all methods and datasets.

**Demonstration of the capabilities of BARLOWDTI<sub>XXL</sub>.** To use BARLOWDTI in real-world applications, more training data is needed to predict meaningful interactions. For this purpose, we have built BARLOWDTI<sub>XXL</sub>, which is trained on more than 3 600 000 curated DTI pairs.<sup>32</sup> We looked at several co-crystal structures as case studies to provide insight into the possibilities using BARLOWDTI<sub>XXL</sub>. In order to demonstrate the ability to generalise beyond the learnt DTIs, we evaluated our approach on structures which are not part of the training set. Our aim is to demonstrate the applicability of the model to multiple structures and affinities, as in the study performed by Dienemann et al.. The importance of this work is further emphasised by its relevance to the malaria-causing parasite *Plasmodium falciparum*.<sup>52</sup>

We first analysed the co-crystal structures *Plasmodium falciparum* lipoate protein ligase 1 LipL1 (5T8U) and *Listeria monocytogenes* lplA1 (8CRI), which share a low sequence identity (28.7 %) despite their structural similarity. Our objective is to evaluate the model’s ability to generalise, particularly when only 1D input is provided. This evaluation focuses on the model’s performance in capturing both biological function and structural attributes under these conditions. Secondly, we examined the predictive shifts induced by ligand methylation and explored the interaction dynamics of a novel enzyme inhibitor C3 (8CRL). This case study is further enriched with isothermal titration calorimetry (ITC) data,<sup>52</sup> offering insights into the ligand’s affinity towards the target proteins.

Our results indicate, that BARLOWDTI<sub>XXL</sub> is able to accurately predict the correlation between the experimentally determined affinity measured via ITC and the likelihood of the DTI (Fig. 3b). These capabilities provide useful insight in the drug discovery process, as researchers are able to



prioritise chemical scaffolds. BARLOWDTI<sub>XXL</sub> is able to catch small changes to the ligands structure and accurately predict the shift in interaction likelihood. This is illustrated by the methylation of lipoic acid (LA), where our method predicts a significant decrease in interaction likelihood, consistent with the decrease in affinity measured by ITC.

We looked at Shapley additive explanation (SHAP) values to examine the influence of each input modality on the model (Fig. 4). Regardless of the ligand molecule chosen, each modality proved equally important for prediction. This finding highlights the functionality and predictive power of BARLOWDTI’s architecture.

**Explaining BARLOWDTI by investigating sample importance.** We analysed the importance of individual samples within the training set to understand how BARLOWDTI classifies DTIs. In Fig. 3d,e, we identified the most influential training pairs by examining those with the highest Jaccard similarity, calculated from the leaf indices of the GBM in BARLOWDTI<sub>XXL</sub>. The most influential training sample is the *Homo sapiens* lipoyl amidotransferase LIPT1 for both lplA1 and LipL1, with LA as the common ligand (Fig. 3a,e). LIPT1 and lplA1 ( $J = 0.909$ ) share a sequence identity of 31.8 %, while LIPT1 and LipL1 ( $J = 0.913$ ) only share 29.7 % (Fig. 6).

To investigate the biochemical implications of the training sample to the model’s prediction, we performed a structural study. We leveraged the availability of crystallographic data to perform in-depth structural analyses on lplA1 (8CRI) and LipL1 (5T8U). A superposition of lplA1 with LIPT1 revealed a root mean square deviation of atomic positions (RMSD) of 2.07 Å, while LipL1 exhibited an RMSD of 1.72 Å. These RMSD values reflect a significant structural congruence among these enzymes, notwithstanding their low sequence identity. Despite this structural similarity, it is noteworthy that human LIPT1 does not catalyse the same reaction as lplA1 and LipL1.<sup>54</sup>

Furthermore, we looked at the active site of LipL1, where all residues are conserved relative to LIPT1 (Fig. 3c). In lplA1, one notable substitution can be observed. L181 in LIPT1 is replaced by M151, possibly explaining the higher Jaccard similarity of LipL1 over lplA1. This conservation pattern underscores a highly conserved binding pocket across species, as confirmed by sequence alignment data. These results highlight the awareness of BARLOWDTI<sub>XXL</sub> to ligand-binding residues and help to understand how the prediction of the model is achieved.

In summary, BARLOWDTI<sub>XXL</sub> effectively learns DTIs by leveraging catalytically active and stabilising residues, demonstrating the model’s ability to generalise from 1D input data. This capability makes BARLOWDTI<sub>XXL</sub> well-suited for applications in drug discovery.

### 3 Conclusions

Our proposed method, BARLOWDTI, integrates sequence information with the Barlow Twins SSL architecture and GBM models, representing a powerful fusion of ML and DL techniques.

Our approach demonstrates state-of-the-art DTI prediction capabilities, validated across multiple benchmarks and data splits. Notably, our method outperforms existing literature benchmarks in ten out of twelve datasets evaluated.

To elucidate the efficacy of BARLOWDTI, we conducted an ablation study to investigate the contribution of its core components and their impact on performance. In addition, we re-evaluated the choice of baselines in numerous publications and advocate the inclusion of GBM baselines. Furthermore, we explored the classification mechanism of BARLOWDTI for DTIs by performing a structure-based analysis of the most influential training samples. This was done by adapting a previously developed influence method to gain deeper insight into training sample importance.

Given the model’s exceptional performance, we are confident that BARLOWDTI can significantly accelerate the drug discovery process and offer significant time and cost savings through the use of virtual screening campaigns. To make BARLOWDTI accessible to the scientific community, we provide an easy to use and free web interface at <https://www.bio.nat.tum.de/oc2/barlowdti>.

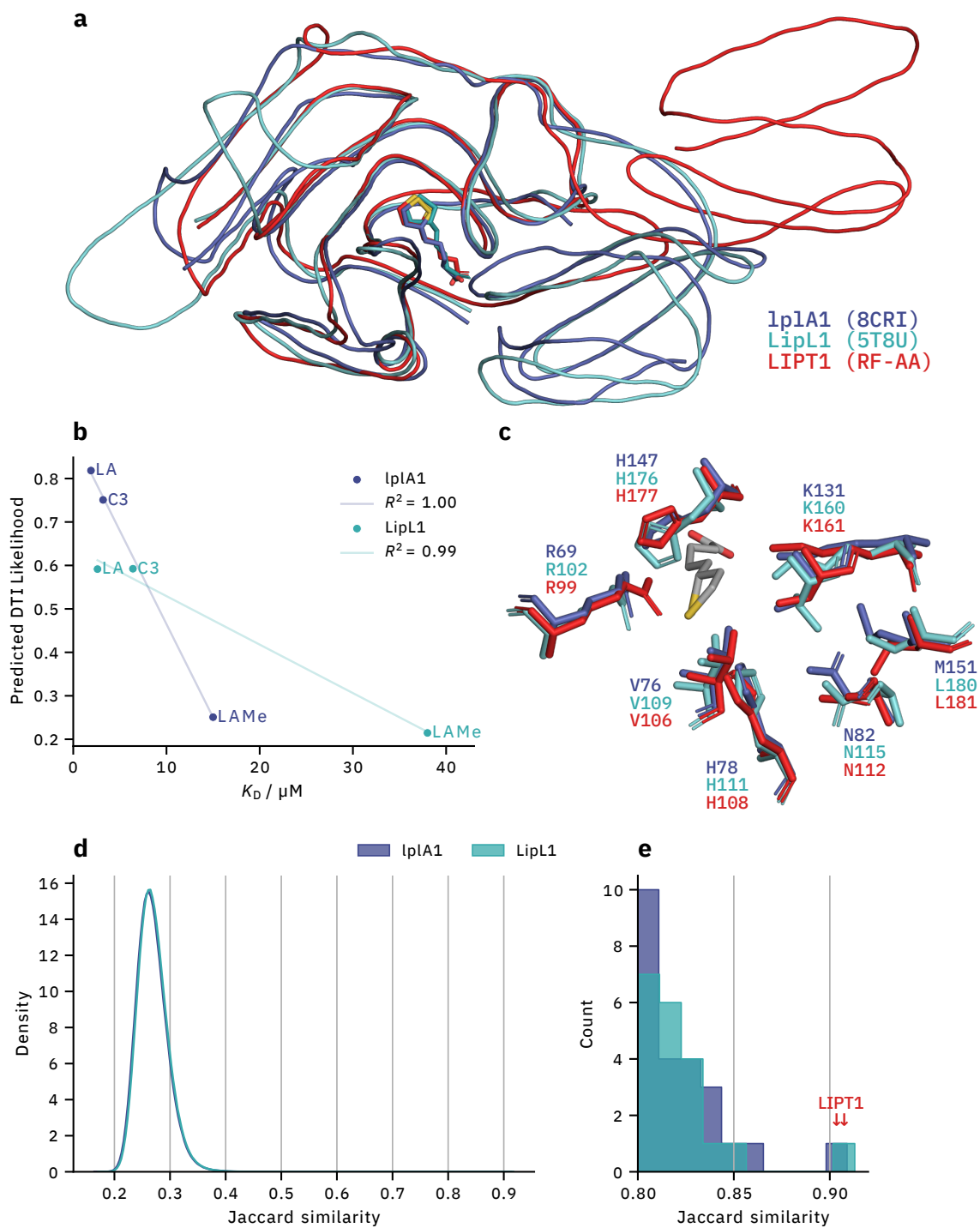


Figure 3: **Structure-based explanation of BARLOWDTI<sub>XXL</sub> predictions.** a) Co-crystal structures of lplA1 and LipL1 with LA as ligand are shown in superposition, together with the most influential training sample. b) The squared Pearson  $R^{53}$  correlation of BARLOWDTI<sub>XXL</sub> and ITC measurements is presented.<sup>52</sup> c) The protein residue–ligand interactions at the active site are compared. d) We identified the most influential training samples for LA predictions. The distribution of Jaccard similarity for all training samples is shown. We applied kernel density estimation to the histogram to improve visibility, due to the large training set size. e) The most influential training samples are highlighted (↓).

## 4 Methods

### 4.1 Datasets

To evaluate the performance of BARLOWDTI, three established benchmarks are used. They all provide fixed splits for training, evaluation and testing. In some publications the training and evaluation is merged to improve predictive performance. To endure comparability, this was not done in this work. All metrics listed from other publications are also listed where only the training set is used.

In addition, Kang et al. first proposed splits for large DTI datasets, BioSNAP,<sup>34</sup> BindingDB<sup>35</sup> and DAVIS.<sup>36,40</sup>

The addition of a variety of splits with an additional benchmark Human<sup>41</sup> are proposed by Koh et al., we evaluate these separately.<sup>16</sup>

For all datasets, to reduce bias and improve model performance, the SMILES are cleaned using the Python ChEMBL curation pipeline.<sup>55</sup> All duplicate and erroneous molecule and protein information that could not be parsed is removed. Training is performed on the predefined training splits.

### 4.2 Representations

**Molecular information.** The SMILES are converted into ECFPs using RDKit.<sup>56</sup> We used them with 1024 bit and a radius of 2.

**Amino acid sequence information.** The amino acid sequences are converted into vectors, by using the PLM ProstT5.<sup>26</sup>

### 4.3 Barlow Twins model configuration

The proposed method is based on the Barlow Twins<sup>30</sup> network architecture, which employs one encoder for each modality and a unified projector. The encoders and projector are multilayer perceptron (MLP) based. The loss function is adapted from the original Barlow Twins publication and enforces cross-correlation between the projections of the modalities.<sup>30</sup>

The BARLOWDTI architecture is coded in Python using PyTorch.<sup>57,58</sup>

**Pre-training Barlow Twins.** Here we pre-train the Barlow Twins architecture on our joint DTI dataset, based on BioSNAP, BindingDB, DAVIS and DrugBank,<sup>37</sup> removing duplicates and without labels to teach DTIs. Early stopping is implemented to avoid overfitting, which is carried out using a 15 % validation split.

**Hyperparameter optimisation** Manual hyperparameter optimisation is performed, shown in Tab. 3.

**Feature-extractor.** When performing feature-extraction, we use the pre-trained BARLOWDTI model. For training and prediction, we extract the embeddings after the encoders for each modality and concatenate them. Finally, a GBM, XGBoost<sup>28</sup> Python implementation, is trained on the embeddings in combination with the labels for each training sets respectively.

**Hyperparameter optimisation** If a benchmark provides a dedicated validation set, this was used for Optuna<sup>59</sup> hyperparameter optimisation. The optimisation was carried out for 100 trials with the parameters shown in Tab. 4.

Table 3: Barlow Twins hyperparameters. The best values are marked in bold.

Hyperparameter	Value / Range
enc_n_neurons	1024, 2048, <b>4096</b>
enc_n_layers	1, 2, 3
proj_n_neurons	1024, <b>2048</b> , 4096
proj_n_layers	<b>1</b> , 2, 3
embedding_dim	512, 1024, 2048
act_function	ReLU
aa_emb_size	1024
loss_weight	$1 \times 10^{-5}$ , <b>0.005</b> , 0.1
batch_size	4096
epochs	250
optimizer	AdamW
learning_rate	$1 \times 10^{-5}$ , <b><math>3 \times 10^{-4}</math></b> , 0.1
beta_1	0.9
beta_2	0.999
weight_decay	$5 \times 10^{-5}$
step_size	10
gamma	0.1
val_split	0.1

Table 4: GBM hyperparameters. Best parameters differ for each benchmarking dataset and split.

Hyperparameter	Value / Range
n_estimators	[100, 1000] (step=100)
learning_rate	[1e-8, 1.0] (log scale)
max_depth	[2, 12]
gamma	[1e-8, 1.0] (log scale)
min_child_weight	[1e-8, 1e2] (log scale)
subsample	[0.4, 1.0]
reg_lambda	[1e-6, 10] (log scale)

#### 4.4 BARLOWDTI<sub>XXL</sub>

We introduce BARLOWDTI<sub>XXL</sub>, a model trained for use in real-world applications. To build BARLOWDTI<sub>XXL</sub>, we curated and standardised the large DTI dataset proposed by Golts et al. (procedure adapted from the ‘‘Datasets’’ section).<sup>32</sup> Furthermore, we used random undersampling with a 3:1 ratio of non-interactors to interactors to improve model generalisation. Then we added the training splits from BioSNAP, BindingDB and DAVIS, resulting in a model trained with 3 653 631 DTI pairs (2 789 498 non-interactors, 864 133 interactors).

BARLOWDTI<sub>XXL</sub> uses the same architecture as BARLOWDTI, using the powerful Barlow Twins network as feature-extraction method in combination with the GBM XGBoost.<sup>28,30</sup>

#### 4.5 Baseline model configuration

As a baseline, we have selected a GBM. Similar to our feature-extraction implementation, for all features we concatenate both ECFP and PLM embeddings. Finally, a GBM, XGBoost Python implementation, is trained on the ECFP and PLM embedding concatenation in combination with the labels for each training set, respectively.

## 4.6 Case study

Amino acid sequence information as well as ligand information is taken from The Protein Data Bank to perform predictions using BARLOWDTI.<sup>60</sup> Complex structures were generated using RoseTTAFold All-Atom.<sup>21</sup>

Sequence identity was determined. Therefore, sequences were aligned using the BLASTP<sup>61,62</sup> algorithm at <https://blast.ncbi.nlm.nih.gov>.<sup>63</sup> PyMOL 2 is used for structure visualisation and RMSD value calculation.<sup>64</sup>

**Explainability based on Shapley additive explanation values.** We applied the TreeExplainer<sup>65,66</sup> algorithm to the GBM of BARLOWDTI<sub>XXL</sub> extracted and visualised the SHAP values.

**Explainability based on sample importance.** To assess how the model decides to classify drug-target pairs as interacting or non-interacting, we looked at the influence of training samples, as similarly proposed by Brophy and Lowd for uncertainty estimation.<sup>33</sup> We used a similar concept but changed the approach to identify the most influential training data. This is done by obtaining the leaf indices of the GBM of all training samples. Then we compare the leaf indices at inference time with the leaf indices of the training samples. Finally, we find the most influential samples by computing the pairwise Jaccard similarity of the leaf index vectors,<sup>67</sup>

$$J(A, B) = \frac{|A \cap B|}{|A \cup B|}.$$

The most influential training sample is represented by the maximum Jaccard similarity.

## 5 Code and Data Availability

The easy-to-use web interface can be found at <https://www.bio.nat.tum.de/oc2/barlowdti>. The code is available on GitHub <https://github.com/maxischuh/BarlowDTI>. Also available on GitHub are the curated and extensive BARLOWDTI<sub>XXL</sub> training, as well as the benchmark data.

The system used for computational work is equipped with an AMD Ryzen Threadripper PRO 5995WX CPU with 64/128 cores/threads and 1024 GB RAM. The server is also powered by an NVIDIA RTX 4090 GPU with 24 GB VRAM.

**Acknowledgements.** The authors thank Merck KGaA Darmstadt for their generous support with the Merck Future Insight Prize 2020. This project is also cofunded by the European Union (ERC, breakingBAC, 101096911). All authors thank Prof. Michael Groll for his insight into the crystal structure data. M.G.S. thanks Joshua Hesse and Aleksandra Daniluk for their valuable input and helpful feedback and Leonard Gareis for assistance with the website.

## References

- [1] Humphrey P. Rang, Maureen M. Dale, James M. Ritter, Rod J. Flower, and Graeme Henderson. *Rang & Dale's Pharmacology*. Elsevier Health Sciences, April 2011. ISBN 978-0-7020-4504-2.
- [2] Stephen M. Strittmatter. Overcoming Drug Development Bottlenecks With Repurposing: Old drugs learn new tricks. *Nature Medicine*, 20(6):590–591, June 2014. ISSN 1546-170X. doi: 10.1038/nm.3595.
- [3] Jp Hughes, S Rees, Sb Kalindjian, and Kl Philpott. Principles of early drug discovery. *British Journal of Pharmacology*, 162(6):1239–1249, 2011. ISSN 1476-5381. doi: 10.1111/j.1476-5381.2010.01127.x.

- [4] Tom L Blundell, Bancinyane L Sibanda, Rinaldo Wander Montalvão, Suzanne Brewerton, Vijayalakshmi Chelliah, Catherine L Worth, Nicholas J Harmer, Owen Davies, and David Burke. Structural biology and bioinformatics in drug design: Opportunities and challenges for target identification and lead discovery. *Philosophical Transactions of the Royal Society B: Biological Sciences*, 361(1467):413–423, February 2006. doi: 10.1098/rstb.2005.1800.
- [5] Christofer S. Tautermann. Current and Future Challenges in Modern Drug Discovery. In Alexander Heifetz, editor, *Quantum Mechanics in Drug Discovery*, pages 1–17. Springer US, New York, NY, 2020. ISBN 978-1-07-160282-9. doi: 10.1007/978-1-0716-0282-9\_1.
- [6] P. C. Agu, C. A. Afiukwa, O. U. Orji, E. M. Ezeh, I. H. Ofoke, C. O. Ogbu, E. I. Ugwuja, and P. M. Aja. Molecular docking as a tool for the discovery of molecular targets of nutraceuticals in diseases management. *Scientific Reports*, 13(1):13398, August 2023. ISSN 2045-2322. doi: 10.1038/s41598-023-40160-2.
- [7] Brian J. Bender, Stefan Gahbauer, Andreas Lutten, Jiankun Lyu, Chase M. Webb, Reed M. Stein, Elissa A. Fink, Trent E. Balius, Jens Carlsson, John J. Irwin, and Brian K. Shoichet. A practical guide to large-scale docking. *Nature Protocols*, 16(10):4799–4832, October 2021. ISSN 1750-2799. doi: 10.1038/s41596-021-00597-z.
- [8] Scott A. Hollingsworth and Ron O. Dror. Molecular Dynamics Simulation for All. *Neuron*, 99(6):1129–1143, September 2018. ISSN 0896-6273. doi: 10.1016/j.neuron.2018.08.011.
- [9] Martin Karplus and Gregory A. Petsko. Molecular dynamics simulations in biology. *Nature*, 347(6294):631–639, October 1990. ISSN 1476-4687. doi: 10.1038/347631a0.
- [10] Ashwin Dhakal, Cole McKay, John J. Tanner, and Jianlin Cheng. Artificial intelligence in the prediction of protein–ligand interactions: Recent advances and future directions. *Briefings in Bioinformatics*, 23(1), January 2022. doi: 10.1093/bib/bbab476.
- [11] Yujie You, Xin Lai, Yi Pan, Huiru Zheng, Julio Vera, Suran Liu, Senyi Deng, and Le Zhang. Artificial intelligence in cancer target identification and drug discovery. *Signal Transduction and Targeted Therapy*, 7(1):1–24, May 2022. ISSN 2059-3635. doi: 10.1038/s41392-022-00994-0.
- [12] Douglas B. Kitchen, Hélène Decornez, John R. Furr, and Jürgen Bajorath. Docking and scoring in virtual screening for drug discovery: Methods and applications. *Nature Reviews Drug Discovery*, 3(11):935–949, November 2004. ISSN 1474-1784. doi: 10.1038/nrd1549.
- [13] Andrew L. Hopkins. Predicting promiscuity. *Nature*, 462(7270):167–168, November 2009. ISSN 1476-4687. doi: 10.1038/462167a.
- [14] Lifan Chen, Xiaoqin Tan, Dingyan Wang, Feisheng Zhong, Xiaohong Liu, Tianbiao Yang, Xiaomin Luo, Kaixian Chen, Hualiang Jiang, and Mingyue Zheng. TransformerCPI: Improving compound–protein interaction prediction by sequence-based deep learning with self-attention mechanism and label reversal experiments. *Bioinformatics*, 36(16):4406–4414, August 2020. ISSN 1367-4803. doi: 10.1093/bioinformatics/btaa524.
- [15] Mingjian Jiang, Zhen Li, Shugang Zhang, Shuang Wang, Xiaofeng Wang, Qing Yuan, and Zhiqiang Wei. Drug–target affinity prediction using graph neural network and contact maps. *RSC Advances*, 10(35):20701–20712, May 2020. ISSN 2046-2069. doi: 10.1039/D0RA02297G.
- [16] Huan Yee Koh, Anh T. N. Nguyen, Shirui Pan, Lauren T. May, and Geoffrey I. Webb. Physicochemical graph neural network for learning protein–ligand interaction fingerprints from sequence data. *Nature Machine Intelligence*, 6(6):673–687, June 2024. ISSN 2522-5839. doi: 10.1038/s42256-024-00847-1.

- [17] Jonghyun Lee, Dae Won Jun, Ildae Song, and Yun Kim. DLM-DTI: A dual language model for the prediction of drug-target interaction with hint-based learning. *Journal of Cheminformatics*, 16(1):1–12, December 2024. ISSN 1758-2946. doi: 10.1186/s13321-024-00808-1.
- [18] Mingjian Jiang, Shuang Wang, Shugang Zhang, Wei Zhou, Yuanyuan Zhang, and Zhen Li. Sequence-based drug-target affinity prediction using weighted graph neural networks. *BMC Genomics*, 23(1):449, June 2022. ISSN 1471-2164. doi: 10.1186/s12864-022-08648-9.
- [19] Gustaf Ahdriz, Nazim Bouatta, Christina Floristean, Sachin Kadyan, Qinghui Xia, William Gerecke, Timothy J. O’Donnell, Daniel Berenberg, Ian Fisk, Niccolò Zanichelli, Bo Zhang, Arkadiusz Nowaczynski, Bei Wang, Marta M. Stepniewska-Dziubinska, Shang Zhang, Adegoke Ojewole, Murat Efe Guney, Stella Biderman, Andrew M. Watkins, Stephen Ra, Pablo Ribalta Lorenzo, Lucas Nivon, Brian Weitzner, Yih-En Andrew Ban, Shiyang Chen, Minjia Zhang, Conglong Li, Shuaiwen Leon Song, Yuxiong He, Peter K. Sorger, Emad Mostaque, Zhao Zhang, Richard Bonneau, and Mohammed AlQuraishi. OpenFold: Retraining AlphaFold2 yields new insights into its learning mechanisms and capacity for generalization. *Nature Methods*, pages 1–11, May 2024. ISSN 1548-7105. doi: 10.1038/s41592-024-02272-z.
- [20] Josh Abramson, Jonas Adler, Jack Dunger, Richard Evans, Tim Green, Alexander Pritzel, Olaf Ronneberger, Lindsay Willmore, Andrew J. Ballard, Joshua Bambrick, Sebastian W. Bodenstein, David A. Evans, Chia-Chun Hung, Michael O’Neill, David Reiman, Kathryn Tunyasuvunakool, Zachary Wu, Akvilė Žemgulytė, Eirini Arvaniti, Charles Beattie, Ottavia Bertolli, Alex Bridgland, Alexey Cherepanov, Miles Congreve, Alexander I. Cowen-Rivers, Andrew Cowie, Michael Figurnov, Fabian B. Fuchs, Hannah Gladman, Rishub Jain, Yousuf A. Khan, Caroline M. R. Low, Kuba Perlin, Anna Potapenko, Pascal Savy, Sukhdeep Singh, Adrian Stecula, Ashok Thillaisundaram, Catherine Tong, Sergei Yakneen, Ellen D. Zhong, Michal Zielinski, Augustin Židek, Victor Bapst, Pushmeet Kohli, Max Jaderberg, Demis Hassabis, and John M. Jumper. Accurate structure prediction of biomolecular interactions with AlphaFold 3. *Nature*, 630(8016):493–500, June 2024. ISSN 1476-4687. doi: 10.1038/s41586-024-07487-w.
- [21] Rohith Krishna, Jue Wang, Woody Ahern, Pascal Sturmfels, Preetham Venkatesh, Indrek Kalvet, Gyu Rie Lee, Felix S. Morey-Burrows, Ivan Anishchenko, Ian R. Humphreys, Ryan McHugh, Dionne Vafeados, Xinting Li, George A. Sutherland, Andrew Hitchcock, C. Neil Hunter, Alex Kang, Evans Brackenbrough, Asim K. Bera, Minkyung Baek, Frank DiMaio, and David Baker. Generalized biomolecular modeling and design with RoseTTAFold All-Atom. *Science*, 384(6693):eadl2528, March 2024. doi: 10.1126/science.adl2528.
- [22] Oleg Trott and Arthur J. Olson. AutoDock Vina: Improving the speed and accuracy of docking with a new scoring function, efficient optimization, and multithreading. *Journal of Computational Chemistry*, 31(2):455–461, 2010. ISSN 1096-987X. doi: 10.1002/jcc.21334.
- [23] Gabriele Corso, Hannes Stärk, Bowen Jing, Regina Barzilay, and Tommi Jaakkola. DiffDock: Diffusion Steps, Twists, and Turns for Molecular Docking, February 2023.
- [24] Xin-heng He, Chong-zhao You, Hua-liang Jiang, Yi Jiang, H. Eric Xu, and Xi Cheng. AlphaFold2 versus experimental structures: Evaluation on G protein-coupled receptors. *Acta Pharmacologica Sinica*, 44(1):1–7, January 2023. ISSN 1745-7254. doi: 10.1038/s41401-022-00938-y.
- [25] Shuangli Li, Jingbo Zhou, Tong Xu, Liang Huang, Fan Wang, Haoyi Xiong, Weili Huang, Dejing Dou, and Hui Xiong. Structure-aware Interactive Graph Neural Networks for the Prediction of Protein-Ligand Binding Affinity. In *Proceedings of the 27th ACM SIGKDD Conference on Knowledge Discovery & Data Mining*, KDD ’21, pages 975–985, New York, NY,

- USA, August 2021. Association for Computing Machinery. ISBN 978-1-4503-8332-5. doi: 10.1145/3447548.3467311.
- [26] Michael Heinzinger, Konstantin Weissenow, Joaquin Gomez Sanchez, Adrian Henkel, Milot Mirdita, Martin Steinegger, and Burkhard Rost. Bilingual Language Model for Protein Sequence and Structure, March 2024.
- [27] Michel van Kempen, Stephanie S. Kim, Charlotte Tumescheit, Milot Mirdita, Jeongjae Lee, Cameron L. M. Gilchrist, Johannes Söding, and Martin Steinegger. Fast and accurate protein structure search with Foldseek. *Nature Biotechnology*, 42(2):243–246, February 2024. ISSN 1546-1696. doi: 10.1038/s41587-023-01773-0.
- [28] Tianqi Chen and Carlos Guestrin. XGBoost: A Scalable Tree Boosting System. In *Proceedings of the 22nd ACM SIGKDD International Conference on Knowledge Discovery and Data Mining*, pages 785–794, August 2016. doi: 10.1145/2939672.2939785.
- [29] Maximilian G. Schuh, Davide Boldini, and Stephan A. Sieber. Synergizing Chemical Structures and Bioassay Descriptions for Enhanced Molecular Property Prediction in Drug Discovery. *Journal of Chemical Information and Modeling*, 64(12):4640–4650, June 2024. ISSN 1549-9596. doi: 10.1021/acs.jcim.4c00765.
- [30] Jure Zbontar, Li Jing, Ishan Misra, Yann LeCun, and Stéphane Deny. Barlow Twins: Self-Supervised Learning via Redundancy Reduction, June 2021.
- [31] Horace B Barlow et al. Possible principles underlying the transformation of sensory messages. *Sensory communication*, 1(01):217–233, 1961.
- [32] Alex Golts, Vadim Ratner, Yoel Shoshan, Moshe Raboh, Sagi Polaczek, Michal Ozery-Flato, Daniel Shats, Liam Hazan, Sivan Ravid, and Efrat Hexter. A large dataset curation and benchmark for drug target interaction, January 2024.
- [33] Jonathan Brophy and Daniel Lowd. Instance-Based Uncertainty Estimation for Gradient-Boosted Regression Trees, October 2022.
- [34] Marinka Zitnik, Rok Sosič, Sagar Maheshwari, and Jure Leskovec. BioSNAP Datasets: Stanford biomedical network dataset collection. <http://snap.stanford.edu/biodata>, August 2018.
- [35] Tiqing Liu, Yuhmei Lin, Xin Wen, Robert N. Jorissen, and Michael K. Gilson. BindingDB: A web-accessible database of experimentally determined protein–ligand binding affinities. *Nucleic Acids Research*, 35(suppl\_1):D198–D201, January 2007. ISSN 0305-1048. doi: 10.1093/nar/gkl999.
- [36] Mindy I. Davis, Jeremy P. Hunt, Sanna Herrgard, Pietro Ciceri, Lisa M. Wodicka, Gabriel Pallares, Michael Hocker, Daniel K. Treiber, and Patrick P. Zarrinkar. Comprehensive analysis of kinase inhibitor selectivity. *Nature Biotechnology*, 29(11):1046–1051, November 2011. ISSN 1546-1696. doi: 10.1038/nbt.1990.
- [37] Craig Knox, Mike Wilson, Christen M Klinger, Mark Franklin, Eponine Oler, Alex Wilson, Allison Pon, Jordan Cox, Na Eun (Lucy) Chin, Seth A Strawbridge, Marysol Garcia-Patino, Ray Kruger, Aadhavya Sivakumaran, Selena Sanford, Rahil Doshi, Nitya Khetarpal, Omolola Fatokun, Daphnee Doucet, Ashley Zubkowski, Dorsa Yahya Rayat, Hayley Jackson, Karxena Harford, Afia Anjum, Mahi Zakir, Fei Wang, Siyang Tian, Brian Lee, Jaanus Liigand, Harrison Peters, Ruo Qi (Rachel) Wang, Tue Nguyen, Denise So, Matthew Sharp, Rodolfo da Silva, Cyrella Gabriel, Joshua Scantlebury, Marissa Jasinski, David Ackerman, Timothy Jewison,



- Tanvir Sajed, Vasuk Gautam, and David S Wishart. DrugBank 6.0: The DrugBank Knowledgebase for 2024. *Nucleic Acids Research*, 52(D1):D1265–D1275, January 2024. ISSN 0305-1048. doi: 10.1093/nar/gkad976.
- [38] Sunghwan Kim, Jie Chen, Tiejun Cheng, Asta Gindulyte, Jia He, Siqian He, Qingliang Li, Benjamin A. Shoemaker, Paul A. Thiessen, Bo Yu, Leonid Zaslavsky, Jian Zhang, and Evan E. Bolton. PubChem 2023 update. *Nucleic Acids Research*, 51(D1):D1373–D1380, January 2023. ISSN 1362-4962. doi: 10.1093/nar/gkac956.
- [39] David Mendez, Anna Gaulton, A Patrícia Bento, Jon Chambers, Marleen De Veij, Eloy Félix, María Paula Magariños, Juan F Mosquera, Prudence Mutowo, Michal Nowotka, María Gordillo-Marañón, Fiona Hunter, Laura Junco, Grace Mugumbate, Milagros Rodriguez-Lopez, Francis Atkinson, Nicolas Bosc, Chris J Radoux, Aldo Segura-Cabrera, Anne Hersey, and Andrew R Leach. ChEMBL: Towards direct deposition of bioassay data. *Nucleic acids research*, 47(D1): D930–D940, January 2019. ISSN 1362-4962. doi: 10.1093/nar/gky1075.
- [40] Hyeunseok Kang, Sungwoo Goo, Hyunjung Lee, Jung-woo Chae, Hwi-yeol Yun, and Sangkeun Jung. Fine-tuning of BERT Model to Accurately Predict Drug–Target Interactions. *Pharmaceutics*, 14(8):1710, August 2022. ISSN 1999-4923. doi: 10.3390/pharmaceutics14081710.
- [41] Kexin Huang, Cao Xiao, Lucas M Glass, and Jimeng Sun. MolTrans: Molecular Interaction Transformer for drug–target interaction prediction. *Bioinformatics*, 37(6):830–836, March 2021. ISSN 1367-4803. doi: 10.1093/bioinformatics/btaa880.
- [42] Rohit Singh, Samuel Sledzieski, Bryan Bryson, Lenore Cowen, and Bonnie Berger. Contrastive learning in protein language space predicts interactions between drugs and protein targets. *Proceedings of the National Academy of Sciences*, 120(24):e2220778120, June 2023. doi: 10.1073/pnas.2220778120.
- [43] Peizhen Bai, Filip Miljković, Bino John, and Haiping Lu. Interpretable bilinear attention network with domain adaptation improves drug–target prediction. *Nature Machine Intelligence*, 5(2):126–136, February 2023. ISSN 2522-5839. doi: 10.1038/s42256-022-00605-1.
- [44] Penglei Wang, Shuangjia Zheng, Yize Jiang, Chengtao Li, Junhong Liu, Chang Wen, Atanas Patronov, Dahong Qian, Hongming Chen, and Yuedong Yang. Structure-Aware Multimodal Deep Learning for Drug–Protein Interaction Prediction. *Journal of Chemical Information and Modeling*, 62(5):1308–1317, March 2022. ISSN 1549-9596. doi: 10.1021/acs.jcim.2c00060.
- [45] Zhenxing Wu, Minfeng Zhu, Yu Kang, Elaine Lai-Han Leung, Tailong Lei, Chao Shen, Dejun Jiang, Zhe Wang, Dongsheng Cao, and Tingjun Hou. Do we need different machine learning algorithms for QSAR modeling? A comprehensive assessment of 16 machine learning algorithms on 14 QSAR data sets. *Briefings in Bioinformatics*, 22(4):bbaa321, July 2021. ISSN 1477-4054. doi: 10.1093/bib/bbaa321.
- [46] Robert P. Sheridan, Wei Min Wang, Andy Liaw, Junshui Ma, and Eric M. Gifford. Extreme Gradient Boosting as a Method for Quantitative Structure–Activity Relationships. *Journal of Chemical Information and Modeling*, 56(12):2353–2360, December 2016. ISSN 1549-9596. doi: 10.1021/acs.jcim.6b00591.
- [47] Amal Asselman, Mohamed Khaldi, and Souhaib Aammou. Enhancing the prediction of student performance based on the machine learning XGBoost algorithm. *Interactive Learning Environments*, 31(6):3360–3379, August 2023. ISSN 1049-4820. doi: 10.1080/10494820.2021.1928235.

- [48] B. L. WELCH. THE GENERALIZATION OF ‘STUDENT’S’ PROBLEM WHEN SEVERAL DIFFERENT POPULATION VARIANCES ARE INVOLVED. *Biometrika*, 34(1-2):28–35, January 1947. ISSN 0006-3444. doi: 10.1093/biomet/34.1-2.28.
- [49] Pauli Virtanen, Ralf Gommers, Travis E. Oliphant, Matt Haberland, Tyler Reddy, David Cournapeau, Evgeni Burovski, Pearu Peterson, Warren Weckesser, Jonathan Bright, Stéfan J. van der Walt, Matthew Brett, Joshua Wilson, K. Jarrod Millman, Nikolay Mayorov, Andrew R. J. Nelson, Eric Jones, Robert Kern, Eric Larson, C. J. Carey, İlhan Polat, Yu Feng, Eric W. Moore, Jake VanderPlas, Denis Laxalde, Josef Perktold, Robert Cimrman, Ian Henriksen, E. A. Quintero, Charles R. Harris, Anne M. Archibald, Antônio H. Ribeiro, Fabian Pedregosa, and Paul van Mulbregt. SciPy 1.0: Fundamental algorithms for scientific computing in Python. *Nature Methods*, 17(3):261–272, March 2020. ISSN 1548-7105. doi: 10.1038/s41592-019-0686-2.
- [50] Yoav Benjamini and Yosef Hochberg. Controlling the False Discovery Rate: A Practical and Powerful Approach to Multiple Testing. *Journal of the Royal Statistical Society. Series B (Methodological)*, 57(1):289–300, 1995. ISSN 0035-9246.
- [51] Ahmed Elnaggar, Michael Heinzinger, Christian Dallago, Ghalia Rehaw, Yu Wang, Llion Jones, Tom Gibbs, Tamas Feher, Christoph Angerer, Martin Steinegger, Debsindhu Bhowmik, and Burkhard Rost. ProtTrans: Toward Understanding the Language of Life Through Self-Supervised Learning. *IEEE Transactions on Pattern Analysis and Machine Intelligence*, 44(10):7112–7127, October 2022. ISSN 1939-3539. doi: 10.1109/TPAMI.2021.3095381.
- [52] Jan-Niklas Dienemann, Shu-Yu Chen, Manuel Hitzenberger, Montana L. Sievert, Stephan M. Hacker, Sean T. Prigge, Martin Zacharias, Michael Groll, and Stephan A. Sieber. A Chemical Proteomic Strategy Reveals Inhibitors of Lipoate Salvage in Bacteria and Parasites. *Angewandte Chemie International Edition*, 62(31):e202304533, 2023. ISSN 1521-3773. doi: 10.1002/anie.202304533.
- [53] Karl Pearson. Note on Regression and Inheritance in the Case of Two Parents. *Proceedings of the Royal Society of London Series I*, 58:240–242, January 1895.
- [54] Xinyun Cao, Lei Zhu, Xuejiao Song, Zhe Hu, and John E Cronan. Protein moonlighting elucidates the essential human pathway catalyzing lipoic acid assembly on its cognate enzymes. *Proceedings of the National Academy of Sciences*, 115(30):E7063–E7072, 2018.
- [55] A. Patrícia Bento, Anne Hersey, Eloy Félix, Greg Landrum, Anna Gaulton, Francis Atkinson, Louisa J. Bellis, Marleen De Veij, and Andrew R. Leach. An open source chemical structure curation pipeline using RDKit. *Journal of Cheminformatics*, 12(1):51, September 2020. ISSN 1758-2946. doi: 10.1186/s13321-020-00456-1.
- [56] Greg Landrum, Paolo Tosco, Brian Kelley, sriniker, gedec, NadineSchneider, Riccardo Vianello, Ric, Andrew Dalke, Brian Cole, AlexanderSavelyev, Matt Swain, Samo Turk, Dan N, Alain Vaucher, Eisuke Kawashima, Maciej Wójcikowski, Daniel Probst, guillaume godin, David Cosgrove, Axel Pahl, JP, Francois Berenger, strets123, JLVarjo, Noel O’Boyle, Patrick Fuller, Jan Holst Jensen, Gianluca Sforna, and DoliathGavid. Rdkit/rdkit: 2020\_03\_1 (Q1 2020) Release. Zenodo, March 2020.
- [57] Guido van Rossum. Python tutorial. (R 9526), January 1995.
- [58] Adam Paszke, Sam Gross, Francisco Massa, Adam Lerer, James Bradbury, Gregory Chanan, Trevor Killeen, Zeming Lin, Natalia Gimelshein, Luca Antiga, Alban Desmaison, Andreas Köpf, Edward Yang, Zach DeVito, Martin Raison, Alykhan Tejani, Sasank Chilamkurthy,

Benoit Steiner, Lu Fang, Junjie Bai, and Soumith Chintala. PyTorch: An Imperative Style, High-Performance Deep Learning Library, December 2019.

- [59] Takuya Akiba, Shotaro Sano, Toshihiko Yanase, Takeru Ohta, and Masanori Koyama. Optuna: A Next-generation Hyperparameter Optimization Framework. In *Proceedings of the 25th ACM SIGKDD International Conference on Knowledge Discovery & Data Mining*, KDD '19, pages 2623–2631, New York, NY, USA, July 2019. Association for Computing Machinery. ISBN 978-1-4503-6201-6. doi: 10.1145/3292500.3330701.
- [60] Helen M. Berman, John Westbrook, Zukang Feng, Gary Gilliland, T. N. Bhat, Helge Weissig, Ilya N. Shindyalov, and Philip E. Bourne. The Protein Data Bank. *Nucleic Acids Research*, 28(1):235–242, January 2000. ISSN 0305-1048. doi: 10.1093/nar/28.1.235.
- [61] Stephen F. Altschul, Warren Gish, Webb Miller, Eugene W. Myers, and David J. Lipman. Basic local alignment search tool. *Journal of Molecular Biology*, 215(3):403–410, October 1990. ISSN 0022-2836. doi: 10.1016/S0022-2836(05)80360-2.
- [62] Stephen F. Altschul, Thomas L. Madden, Alejandro A. Schäffer, Jinghui Zhang, Zheng Zhang, Webb Miller, and David J. Lipman. Gapped BLAST and PSI-BLAST: A new generation of protein database search programs. *Nucleic Acids Research*, 25(17):3389–3402, September 1997. ISSN 0305-1048. doi: 10.1093/nar/25.17.3389.
- [63] Eric W Sayers, Evan E Bolton, J Rodney Brister, Kathi Canese, Jessica Chan, Donald C Comeau, Ryan Connor, Kathryn Funk, Chris Kelly, Sunghwan Kim, Tom Madej, Aron Marchler-Bauer, Christopher Lanczycki, Stacy Lathrop, Zhiyong Lu, Françoise Thibaud-Nissen, Terence Murphy, Lon Phan, Yuri Skripchenko, Tony Tse, Jiyao Wang, Rebecca Williams, Barton W Trawick, Kim D Pruitt, and Stephen T Sherry. Database resources of the national center for biotechnology information. *Nucleic Acids Research*, 50(D1):D20–D26, January 2022. ISSN 0305-1048. doi: 10.1093/nar/gkab1112.
- [64] Schrödinger, LLC. The PyMOL molecular graphics system, version 1.8. November 2015.
- [65] Scott M Lundberg and Su-In Lee. A Unified Approach to Interpreting Model Predictions. In *Advances in Neural Information Processing Systems*, volume 30. Curran Associates, Inc., 2017.
- [66] Scott M. Lundberg, Gabriel Erion, Hugh Chen, Alex DeGrave, Jordan M. Prutkin, Bala Nair, Ronit Katz, Jonathan Himmelfarb, Nisha Bansal, and Su-In Lee. From local explanations to global understanding with explainable AI for trees. *Nature Machine Intelligence*, 2(1):56–67, January 2020. ISSN 2522-5839. doi: 10.1038/s42256-019-0138-9.
- [67] Paul Jaccard. Étude comparative de la distribution florale dans une portion des Alpes et du Jura. *Bulletin de la Société Vaudoise des Sciences Naturelles*, 37(142):547, 1901. ISSN 0037-9603. doi: 10.5169/seals-266450.
- [68] Frank Wilcoxon. Individual Comparisons by Ranking Methods. *Biometrics Bulletin*, 1(6):80–83, 1945. ISSN 0099-4987. doi: 10.2307/3001968.

## A Additional Results and Discussion

**Statistical testing.** We focus on PR AUC as our metric because it is an established performance indicator in unbalanced scenarios. Secondly, it shows a more pronounced separation between different methods, as most methods show very high values of ROC AUC.

We apply the two-sided Welch’s  $t$ -test,<sup>48,49</sup> with Benjamini-Hochberg<sup>50</sup> multiple test correction. This is done for all methods for which the required performance information exists in the published literature.

In Fig. 2, our primary focus is on the overall change in performance. We therefore make comparisons across all datasets collectively rather than individually. Detailed individual comparisons are provided in Tabs. 1 and 2.

Table 5: Statistical testing of benchmarking BARLOWDTI against other models using Kang et al. splits.<sup>40</sup> Five replicates were performed. Two-sided Welch’s  $t$ -test,<sup>48,49</sup>  $\alpha = 0.001$  with Benjamini-Hochberg<sup>50</sup> multiple test correction was applied.

Dataset	Model	ROC AUC		PR AUC	
		$p_{\text{corr}}$ value	Significant	$p_{\text{corr}}$ value	Significant
BioSNAP	XGBoost	$5.63 \times 10^{-9}$	True	$4.06 \times 10^{-9}$	True
	MolTrans <sup>41</sup>	$1.70 \times 10^{-7}$	True	$4.48 \times 10^{-6}$	True
	Kang et al.	$6.49 \times 10^{-5}$	True	$3.37 \times 10^{-5}$	True
	DLM-DTI <sup>17</sup>	$4.26 \times 10^{-6}$	True	$3.65 \times 10^{-5}$	True
	ConPLex <sup>42</sup>	—	—	$5.77 \times 10^{-10}$	True
BindingDB	XGBoost	$3.45 \times 10^{-7}$	True	$1.89 \times 10^{-6}$	True
	MolTrans <sup>41</sup>	$3.45 \times 10^{-7}$	True	$1.89 \times 10^{-6}$	True
	Kang et al.	$1.70 \times 10^{-6}$	True	$1.19 \times 10^{-5}$	True
	DLM-DTI <sup>17</sup>	$1.58 \times 10^{-4}$	True	$1.89 \times 10^{-6}$	True
	ConPLex <sup>42</sup>	—	—	$2.84 \times 10^{-5}$	True
DAVIS	XGBoost	$6.78 \times 10^{-7}$	True	$5.79 \times 10^{-8}$	True
	MolTrans <sup>41</sup>	$2.89 \times 10^{-7}$	True	$3.74 \times 10^{-5}$	True
	Kang et al.	$6.78 \times 10^{-7}$	True	$1.41 \times 10^{-6}$	True
	DLM-DTI <sup>17</sup>	$6.78 \times 10^{-7}$	True	$3.00 \times 10^{-5}$	True
	ConPLex <sup>42</sup>	—	—	$1.82 \times 10^{-4}$	True

Table 6: Statistical testing of ablation benchmark with BARLOWDTI against other models using Kang et al. splits.<sup>40</sup> Five replicates each are performed. Two-sided Welch’s  $t$ -test,<sup>48,49</sup>  $\alpha = 0.0001$  with Benjamini-Hochberg<sup>50</sup> multiple test correction was applied. (o.: optimised; n.o.: non-optimised)

Comparison		PR AUC	
Model 1	Model 2	$p_{\text{corr}}$ value	Significant
XGBoost	XGBoost o.	$1.47 \times 10^{-7}$	True
XGBoost	BARLOWDTI n.o.	$2.37 \times 10^{-23}$	True
XGBoost	BARLOWDTI	$6.32 \times 10^{-25}$	True
XGBoost o.	BARLOWDTI n.o.	$1.64 \times 10^{-10}$	True
XGBoost o.	BARLOWDTI	$9.48 \times 10^{-15}$	True
BARLOWDTI n.o.	BARLOWDTI	$1.70 \times 10^{-15}$	True

Table 7: Statistical testing of benchmarking BARLOWDTI against other models using Kang et al. splits.<sup>40</sup> For XGBoost five replicates were performed. Two-sided Welch's  $t$ -test,<sup>48,49</sup>  $\alpha = 0.05$  with Benjamini-Hochberg<sup>50</sup> multiple test correction was applied.

Comparison		PR AUC	
Model 1	Model 2	$p_{\text{corr}}$ value	Significant
XGBoost	DLM-DTI	0.1452	False
XGBoost	MolTrans	0.1452	False
XGBoost	Kang et al.	0.1452	False
DLM-DTI	MolTrans	0.7970	False
DLM-DTI	Kang et al.	0.7970	False
MolTrans	Kang et al.	0.7970	False

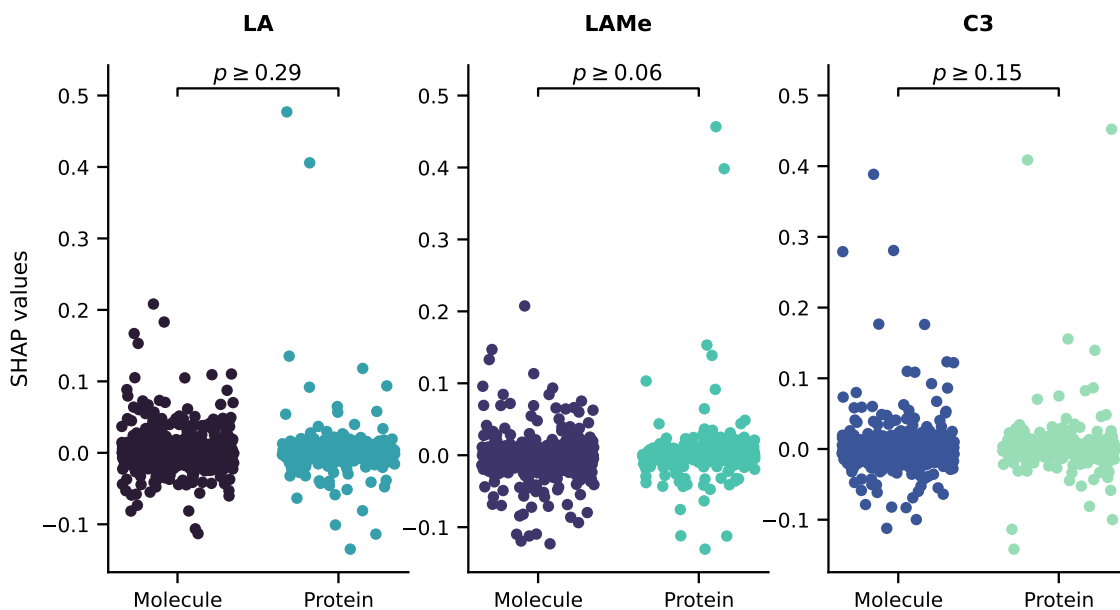


Figure 4: SHAP values of BARLOWDTI<sub>XXL</sub> input modalities. No significant change in distribution could be shown, independent of the ligand molecule, case study based on the Dienemann et al. publication.<sup>52</sup> A two-sided Wilcoxon<sup>68</sup> signed-rank test was applied and respective  $p$ -values are presented within the figure.

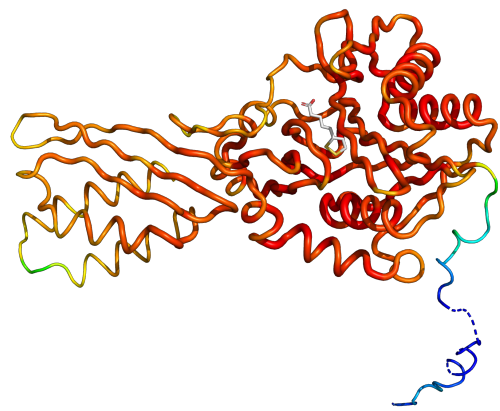


Figure 5: *B* factor visualisation of RoseTTAFold All-Atom<sup>21</sup> prediction of LIPT1.

```

                                1      10      20
lplA1 .....MYFDDNNEKDPRINABFILTELN..
LipL1 .....MKRIFRLVRRCHYSTERRTNGPLVSNQ..NIHFSLENFLNNYDL
LIPT1 MLIPFSKKNCFQLLNCQVFAAGFKKTVKNGLIQSL..DVYQALDLHDHM..

                                30      40      50      60      70
lplA1 .....LDEPLFYIKSTICRNQNTVESIDTEYVEKNDVIVRRLSGGAV
LipL1 LKYLININIEKFNEELRNSIGNNTVSCNKKIKEGVLARRTGGAV
LIPT1 .....LEGRPEFWQSPSVICHQNPWCNLNLMREEGKLARRSGGAV

                                80      90      100     110     120     130
lplA1 VHDGNINFEERDDGESFHNFAKTGFVARRLGVNLRLGNDLDGFFVS
LipL1 VHDGNINFEERDDGESFHNFAKTGFVARRLGVNLRLGNDLDGFFVS
LIPT1 VHDGNINFEERDDGESFHNFAKTGFVARRLGVNLRLGNDLDGFFVS

                                140     150     160     170     180     190
lplA1 GHAFATGKMPSCIINDLNDVAASKPRKKIESKGIKVRSRVANSDFMDQEV
LipL1 GHAFATGKMPSCIINDLNDVAASKPRKKIESKGIKVRSRVANSDFMDQEV
LIPT1 GHAFATGKMPSCIINDLNDVAASKPRKKIESKGIKVRSRVANSDFMDQEV

                                200
lplA1 HESFRDLLLYIFGV.....
LipL1 CENLCIALIKEFTKFYEQNYKENINNIKNLENNINNSFNFQNKEINNTNENNLINNT
LIPT1 HESFRDLLLYIFGV.....

                                210     220     230     240     250     260
lplA1 ...EKVEDVVEYKLTAADWEKIHEISAKRYGNNNYGKSKFDLTRTKRFFVGAV..
LipL1 ...EKFNDITVHIDQNNITKNFELKYNLKDNNYGKSKFDLTRTKRFFVGAV..
LIPT1 .....DNHELINEDELFFGINSKAKELQNNYGKSKFDLTRTKRFFVGAV..

                                270     280     290     300     310     320
lplA1 ...DRLNVQKGHEDIKFGDFFGVKNVADIEEKLVNTTYKREVLAEALVDIDVKEYFGN
LipL1 ...ELFFNSGHEDIKFGDFFGVKNVADIEEKLVNTTYKREVLAEALVDIDVKEYFGN
LIPT1 EIKVFIDKNGREICNEAPDHWLPLEIRDKLNSSLIGSKFCPTETTMLNILRTCPQ

                                330
lplA1 ITKDEFLLDLY.....
LipL1 LDEVRSWILQEL.....
LIPT1 DHKLSKWNILCEKIRGIM

```

Figure 6: Sequence alignment of lplA1, LipL1 and LIPT1.